

Contents lists available at [ScienceDirect](http://www.sciencedirect.com)

Journal of Quantitative Spectroscopy & Radiative Transfer

journal homepage: www.elsevier.com/locate/jqsrt

ACE-FTS ozone, water vapour, nitrous oxide, nitric acid, and carbon monoxide profile comparisons with MIPAS and MLS



Patrick E. Sheese^a, Kaley A. Walker^{a,b,*}, Chris D. Boone^b, Peter F. Bernath^c, Lucien Froidevaux^d, Bernd Funke^e, Piera Raspollini^f, Thomas von Clarmann^g

^a University of Toronto, Department of Physics, 60 St. George St., Toronto, ON, Canada M5S 1A7

^b University of Waterloo, Department of Chemistry, 200 University Ave. W, Waterloo, ON, Canada N2L 3G1

^c Old Dominion University, Department of Chemistry & Biochemistry, 4541 Hampton Boulevard, Norfolk, VA 23529-0126, USA

^d Jet Propulsion Laboratory, 4800 Oak Grove Dr, Pasadena, CA 91109, USA

^e Instituto de Astrofísica de Andalucía, CSIC, Apartado 3004, 18080 Granada, Spain

^f Institute of Applied Physics "Nello Carrara", National Research Council, Via Madonna del Piano 10, 50019 Florence, Italy

^g Karlsruhe Institute of Technology, Institute for Meteorology and Climate Research, H.-v.-Helmholtz-Platz 1, 76344 Karlsruhe, Germany

ARTICLE INFO

Article history:

Received 4 February 2016

Received in revised form

16 June 2016

Accepted 16 June 2016

Available online 24 June 2016

Keywords:

ACE-FTS

MIPAS

MLS

Profile comparison

Stratospheric and mesospheric trace gases

Satellite limb sounding

ABSTRACT

The atmospheric limb sounders, ACE-FTS on the SCISAT satellite, MIPAS on ESA's Envisat satellite, and MLS on NASA's Aura satellite, take measurements used to retrieve atmospheric profiles of O₃, N₂O, H₂O, HNO₃, and CO. Each was taking measurements between February 2004 and April 2012 (ACE-FTS and MLS are currently operational), providing hundreds of profile coincidences in the Northern and Southern hemispheres, and during local morning and evening. Focusing on determining diurnal and hemispheric biases in the ACE-FTS data, this study compares ACE-FTS version 3.5 profiles that are collocated with MIPAS and MLS, and analyzes the differences between instrument retrievals for Northern and Southern hemispheres and for local morning and evening data. For O₃, ACE-FTS is typically within $\pm 5\%$ of mid-stratospheric MIPAS and MLS data and exhibits a positive bias of ~ 10 to 20% in the upper stratosphere – lower mesosphere. For H₂O, ACE-FTS exhibits an average bias of -5% between 20 and 60 km. For N₂O, ACE-FTS agrees with MIPAS and MLS within -20 to $+10\%$ up to 45 km and 35 km, respectively. For HNO₃, ACE-FTS typically agrees within $\pm 10\%$ below 30 km, and exhibits a positive bias of ~ 10 to 20% above 30 km. With respect to MIPAS CO, ACE-FTS exhibits an average -11% bias between 28 and 50 km, and at higher altitudes a positive bias on the order of 10% ($> 100\%$) in the winter (summer). With respect to winter MLS CO, ACE-FTS is typically within $\pm 10\%$ between 25 and 40 km, and has an average bias of -11% above 40 km.

© 2016 Elsevier Ltd. All rights reserved.

1. Introduction

Satellite remote sounding of the Earth's limb is currently the only method of observing the atmosphere that allows for

near-global time series of atmospheric profiles from the upper troposphere to the lower thermosphere. However, each atmospheric limb sounder has its own sources of uncertainty and systematic biases. To get a true understanding of the state of the global atmosphere, these uncertainties and biases must be identified and characterized. Limb sounding instruments can exhibit different systematic differences from similar instruments depending on

* Corresponding author at: University of Toronto, Department of Physics, 60 St. George St., Toronto, ON, Canada M5S 1A7.

E-mail address: kwalker@atmos.physics.utoronto.ca (K.A. Walker).

the observed latitudinal region and/or the observed local time. These biases must also be identified and characterized.

The Atmospheric Chemistry Experiment – Fourier Transform Spectrometer (ACE-FTS) instrument [1] on the SCISAT satellite is a solar occultation limb sounder that has extensive measurement overlap, both spatially and temporally, with the Michelson Interferometer for Passive Atmospheric Sounding (MIPAS) instrument [2,3] on the Envisat satellite and the Microwave Limb Sounder (MLS) [4] on the Aura satellite. There are many hundreds of coincident measurements, in both the Northern and Southern hemispheres, covering the local morning and local evening, between ACE-FTS and both MIPAS and MLS, which are needed for determining any hemispheric and/or diurnal biases between the data sets. These instruments were chosen not only because they have extensive temporal overlap, but because they also retrieve many of the same atmospheric species. The five species they have in common are ozone, water vapour, nitrous oxide, nitric acid, and carbon monoxide. A complete overview of the roles of each of these important species in the different regions of the atmosphere is given by [5], and what follows is a brief synopsis.

Ozone (O_3) is one of the most important atmospheric constituents, as it absorbs harmful solar UV radiation, shielding living organisms on the Earth's surface. Ozone also plays a minor role as a greenhouse gas in the troposphere. Continuous monitoring of vertically-resolved O_3 is therefore vital for understanding O_3 depletion, long-term O_3 recovery, and, to a lesser extent, climate change.

Water vapour (H_2O) is the most important non-anthropogenic greenhouse gas in the Earth's atmosphere, and as such, it has a major influence on the lower atmospheric climate, chemistry, and energy budget. In the middle atmosphere, due to its long lifetime, it is often used as a dynamical tracer. The Brewer–Dobson circulation transports H_2O -rich air from tropospheric low latitudes to stratospheric mid latitudes. Water vapour is also produced in the middle atmosphere via the oxidation of CH_4 and is destroyed via photodissociation as well as via reactions with $O(^1D)$. The middle atmospheric sources and sinks tend to balance near the stratopause region, leading to a climatological H_2O peak in this region.

Nitrous oxide (N_2O) is a minor greenhouse gas, and in the stratosphere it is often used as a dynamical tracer. Moreover, it is the primary source of NO_x in the stratosphere. Stratospheric N_2O typically originates from the surface from different emission sources—agricultural, industrial, biomass burning, etc.—and is distributed throughout the middle atmosphere via the Brewer–Dobson circulation. Recently, it has been discovered that energetic particle precipitation in the upper atmosphere also produces N_2O , which can be transported down into the winter upper stratosphere – lower mesosphere (USLM) [6,7]. Once in the mid stratosphere, N_2O is destroyed by photodissociation and through reactions with $O(^1D)$, producing NO , which catalytically destroys O_3 .

Nitric acid (HNO_3) can remove NO_y from the stratosphere. The main production mechanism for HNO_3 is the three-body reaction between NO_2 , OH , and an air molecule, and the main destruction mechanisms are photolysis

in the UV and through reactions with OH . In the polar winter, N_2O_5 and $ClONO_2$ can react with H_2O or HCl on the surface of polar stratospheric cloud (PSC) particles, producing HNO_3 and chlorine molecules, which then lead to active chlorine species. HNO_3 is typically sequestered by the PSC particles, and subsequent sedimentation of the HNO_3 -containing particles can effectively remove NO_y from the stratosphere.

Carbon monoxide (CO) is a major pollutant and short-lived greenhouse gas in the troposphere. The main sources of CO in the lower atmosphere are surface emissions from fossil fuel combustion and biomass burning, and from hydrocarbon oxidation. In the stratosphere, CH_4 oxidation is the major source of CO and is more effective during sunlit hours, as the two main pathways to creating CO via CH_4 oxidation involve photolysis. In the USLM CO_2 photodissociation directly produces CO , and winter descent from the upper atmosphere also transports in CO -rich air. In the mesosphere and lower thermosphere, where CO is often used as a dynamical tracer, CO is primarily produced via CO_2 photodissociation. Throughout the atmosphere, CO is predominantly lost through chemical reactions with OH .

The following section gives an overview of the ACE-FTS, MIPAS, and MLS instruments, as well as the retrieval algorithms used to derive the data sets analyzed in this study, and Section 3 discusses the methodology used to compare the atmospheric data sets. Section 4 discusses the comparison results and the differences within those results due to diurnal and hemispheric biases. A summary is provided in the final section.

2. Instrumentation

2.1. ACE-FTS on SCISAT

The ACE-FTS instrument is a solar occultation Fourier transform spectrometer operating in the 750 to 4400 cm^{-1} spectral region, with a 0.02 cm^{-1} spectral resolution. It was launched into a high-inclination orbit in August 2003, and since February 2004, ACE-FTS has been providing temperature, pressure, and volume mixing ratio (VMR) profiles of over 30 atmospheric trace gases and over 20 subsidiary isotopologues. Twice per orbit, during sunrise and sunset, ACE-FTS takes measurements approximately every 2 s. Profiles are measured between ~5 and 150 km, with a vertical field of view of ~3 to 4 km and a vertical sampling of ~2 to 6 km, depending on the angle between the satellite's orbital plane and the look direction to the sun.

The ACE-FTS trace species VMR retrieval algorithm is described by [8], and the changes for the most recent version of the retrieval, version 3.5 (v3.5), are detailed by [9]. The retrieval algorithm uses a non-linear least-squares global-fitting technique that fits the ACE-FTS observed spectra in given microwindows to forward modeled spectra—based on line strengths and line widths from the HITRAN 2004 database [10] (with updates as described by [9]). The pressure and temperature profiles used in the forward model are the ACE-FTS derived profiles, calculated by fitting CO_2 lines in the observed spectra. The main

changes made in the v3.5 retrievals are: amended microwindows for the majority of species that now allow for a greater number of interfering species; improvements to the temperature and pressure retrievals, leading to fewer instances of unnatural oscillations in the vertical profiles; and the addition of COCl₂, COClF, H₂CO, CH₃OH, and HCFC-141b to the retrieved profiles, as well as the removal of ClO.

The O₃ retrievals are limited to altitudes between 5 and 95 km. The O₃ retrieval uses 40 microwindows between 829 and 2673 cm⁻¹ and allows for the interfering species CFC-12, HCFC-22, CFC-11, N₂O, CH₄, HCOOH, CO₂, and various isotopologues in the troposphere and stratosphere. ACE-FTS v2.2 updated O₃ was validated by [11], using over 20 different correlative data sets, including satellite, balloon-borne and ground-based observations. It was found that in the lower to mid stratosphere ACE-FTS typically exhibited a positive bias on the order of 1–8%, and in the USLM, the ACE-FTS positive bias was on average ~20%.

The H₂O retrievals are limited to altitudes between 5 and 101 km. The retrieval uses 54 microwindows spanning 937 to 2993 cm⁻¹ and includes CO₂, O₃, N₂O, CH₄, COF₂, and various isotopologues as interfering species. The quality of the v2.2 H₂O data set was assessed by [12], who determined that from the lower stratosphere up into the mesosphere ACE-FTS tended to exhibit a positive bias of ~3 to 10% with respect to correlative data sets. Due to the large variability in water vapour concentration in the upper troposphere, no conclusions as to the quality of the ACE-FTS H₂O data product in this region were drawn [12].

Profiles of N₂O are retrieved between altitudes of 5 and 95 km, using 62 microwindows that range from 829 to 2241 cm⁻¹. Interfering species in the N₂O retrievals include HCFC-22, CH₄, H₂O, O₃, CO, CO₂, HNO₃, and various isotopologues. The ACE-FTS v2.2 N₂O data set was validated by comparing the ACE-FTS data set to correlative data from airborne and satellite based instruments [13]. It was found that below 30 km, ACE-FTS typically agreed with coincident limb sounder data to within 15–20%, and in the 30–50 km region, ACE-FTS typically exhibited a negative bias of about –20 to –50%.

The HNO₃ retrievals use 41 microwindows between 865 and 1978 cm⁻¹ and includes, at different altitudes, the interfering species CFC-12, H₂O, CO₂, OCS, and O₃. The retrieval has a lower and upper altitude limit of 5 km and 62 km, respectively. ACE-FTS v2.2 HNO₃ was validated by [14], who found that the ACE-FTS data and correlative data sets typically agreed within ±20% between altitudes of 18 and 35 km. ACE-FTS data tended to agree best with previous versions of MIPAS and MLS data, with the data sets typically agreeing within ±10% in approximately the same altitude range.

Profiles of CO are retrieved between altitudes of 5 and 110 km. The retrieval uses 40 microwindows within the spectral range of 1950–4285 cm⁻¹, and CO₂, H₂O, O₃, and OCS are included as interfering species. ACE-FTS v2.2 CO profiles have previously been compared to collocated data from satellite and airborne instruments [15]. It was determined that throughout the stratosphere and mesosphere the ACE-FTS data typically agreed with correlative

Table 1

Summary of previously reported ACE-FTS v2.2+ updates systematic biases for O₃, H₂O, N₂O, HNO₃, and CO.

Species	Altitude	Mean bias (%)	Reference
O ₃	Low to mid stratosphere	+1 to +8	[11]
	USLM	~ +20	
H ₂ O	Above hygropause	+3 to +8	[12]
N ₂ O	< 30 km	± 20	[13]
	30–50 km	–20 to –50	
HNO ₃	18–35 km (Compared to MIPAS and MLS)	± 10%	[14]
CO	Throughout stratosphere and mesosphere	± 30%	[15]

measurements to within approximately 25–30%. A known issue with the ACE-FTS CO data product (v3.5 and earlier versions) is that between ~20 and 50 km, the retrieved CO concentrations occasionally spike to large negative values. This is due to large CO variations along the instrument line of sight that are not accounted for in the retrieval. These large negative values are not excluded from the analysis as not to skew the mean.

Table 1 shows a summary of the previously reported ACE-FTS v2.2 biases for O₃, H₂O, N₂O, HNO₃, and CO. All ACE-FTS data used in this study were screened using version 1.1 of the v3.5 quality flags [16]. As such, profiles that contained any physically unrealistic outliers (at any altitude) or were known to be affected by instrument or processing errors were excluded prior to analysis.

2.2. MIPAS on Envisat

The Envisat satellite was launched into a polar, sun synchronous orbit in March 2002, at an altitude of ~800 km and with an ascending node of 22:00 local time (LT). Multiple limb sounding instruments were on board, including the MIPAS instrument. In April 2012, ground control lost communication with Envisat and therefore observational data are no longer accessible.

MIPAS was a Fourier transform spectrometer that observed atmospheric emissions in the Earth's limb between altitudes of 6 and 70 km in its normal observation mode, and up to 170 km in other observation modes, with a vertical field of view of 3 km and a vertical sampling of 1.5–5 km, with ~1400 measurement profiles each day. The spectrometer used five different bands within the spectral window of 685–2410 cm⁻¹ in order to retrieve concentrations of over 20 atmospheric trace species.

In 2004, an anomaly was detected in the MIPAS interferometer drive unit. It was determined that it was necessary to downgrade the full spectral resolution of 0.025 cm⁻¹ with a sampling time of 4.5 s to a resolution of 0.0625 cm⁻¹ with a sampling time of 1.8 s [17]. The reduced sampling time allowed for better vertical sampling. MIPAS operated in this new mode from January 2005 onward, and this study only uses these data in order to avoid any discontinuities that would arise from using data from both resolution modes.

Two different algorithms for retrieving MIPAS level 2 data are used in this study. One was developed by the

European Space Agency (ESA), and the other was developed in collaboration between the Institut für Meteorologie und Klimaforschung at the Karlsruhe Institute of Technology and the Instituto de Astrofísica de Andalucía (IMK-IAA). The ESA algorithm that produces the level 2 retrievals, now on its sixth version (v6; used in this study), is described by [17]. The algorithm fits measured infrared spectra in species-dependent microwindows to a forward modeled spectrum via least squares global-fitting, using the Levenberg–Marquardt method to minimize the fit residual and to regularize the retrieval. The forward model used in the algorithm assumes horizontal homogeneity for all species as well as for temperature, and it assumes that the atmosphere is in local thermodynamic equilibrium (LTE). The regularization of the Levenberg–Marquardt method is controlled by the convergence criteria and is deliberately kept weak. Resulting oscillations within the retrieved profiles are damped a posteriori with a retrieval error dependent regularization strength. The regularization is applied for all species except water vapour since the strength of the regularization, driven by a single altitude-independent parameter, is not suitable to regularize water vapour profiles that vary by two orders of magnitude across the MIPAS retrieval range [17]. The MIPAS ESA algorithm does not include a CO retrieval.

The IMK-IAA algorithm producing level 2 data is now in its fifth version (v5; used in this study) [18]. The IMK-IAA algorithm uses Tikhonov regularization [19] on species-dependent sets of microwindows, which is a constrained iterative inversion technique. The data are retrieved on a 1-km grid, and the altitude-dependent strength of the smoothing constraint was chosen in order to optimize vertical resolution while limiting unphysical oscillations in the retrieved profile. MIPAS IMK-IAA CO and H₂O retrievals are performed in log(VMR) space. The forward model allows for variation in temperature along the line of sight and assumes horizontal homogeneity for all species except CO, for which a line of sight concentration gradient is retrieved jointly. The forward model also allows non-LTE effects which have been accounted for in the retrieval of CO. For other species, LTE is assumed and selected microwindows were determined with the intent to limit non-LTE effects.

All recommended quality, status, and convergence flags were used to screen the MIPAS data sets prior to analysis. The vertical resolution at each altitude for each species was determined as the full-width half-maximum of the corresponding averaging kernels.

2.3. MLS on Aura

The Microwave Limb Sounder on the Aura satellite was launched in July 2004 into a polar, sun synchronous orbit, near 700 km, with an ascending node of 13:45 LT. The MLS instrument uses seven radiometers to measure thermal emission in the Earth's limb within the spectral range of 118 GHz to 2.5 THz. At a rate of one vertical scan every 25 s, MLS obtains nearly 3500 measurement profiles each day. These measurements are used to retrieve vertical profiles, on a fixed pressure grid, of temperature, geopotential height, and concentrations of over 15 atmospheric trace species.

MLS retrieval version 3.3/3.4 is used in this study. The algorithm [20] uses the Newtonian iteration optimal estimation technique [21] with a regularization constraint in altitude regions where the vertical resolution is less than 6 km. However, in cases where the inverse problem is highly non-linear, the Levenberg–Marquardt optimal estimation technique [21] is used. Since successive MLS measurement scans typically sample common volumes of air within their lines of sight, the retrieval algorithm retrieves solutions to successive scans in batches, and within a batch, the state of the atmosphere used for one profile can influence the solutions for neighboring profiles.

All MLS data used in this study have been limited to the recommended pressure limits and were screened using the recommended quality and convergence flags [22]. In the case of HNO₃, both the 240 and 190 GHz channel flags were used. As recommended, data with corresponding negative precision values, indicating poor retrieval response, have not been used. As well, no profiles, of any species, that were flagged as being contaminated by clouds were used in the analysis. The vertical resolution profiles for each species were assumed to be constant for all retrievals, and were calculated as the full-widths at half-maximum of the mean averaging kernel matrices.

3. Methodology

In order to determine if the ACE-FTS data exhibit any diurnal or hemispheric biases, a large sample of coincident profiles between ACE-FTS and the other data sets was necessary in the Northern hemisphere, Southern hemisphere, local morning (AM), and local evening (PM). To facilitate this, the coincidence criteria of requiring observations being made within 3 h and within 350 km of each other was chosen for all comparisons (unless stated otherwise). All VMR profiles used in this study have been spline-interpolated onto the ACE-FTS 1-km grid, ranging from 0.5 to 149.5 km. For the MLS data, the interpolation was done using the measured MLS geopotential heights. In cases where an ACE-FTS measurement was coincident with multiple profiles from another data set, only the profile measured closest in latitude to the ACE-FTS occultation was used. Fig. 1 shows example latitudinal and local time coverage of the ACE-FTS measurements coincident with MIPAS and MLS (within 3 h and 350 km); specifically, all coincident H₂O profile locations with MIPAS ESA and MLS data. It can be seen that the overwhelming majority of coincident profiles are at latitudes poleward of 45°.

In order to limit the effect of biasing comparisons due to differences between the instrument/retrieval vertical resolutions, coincident VMR profiles were vertically smoothed prior to analysis. The profile with finer vertical resolution, X_f , was smoothed by taking a weighted-average of the VMR profile at each altitude level using a weighting function of a normalized Gaussian distribution.

$$X_f^{smooth}(h) = \frac{\int X_f(z)G(h, z)dz}{\int G(h, z)dz}, \quad (1)$$

where h is the altitude level on the ACE-FTS 1-km grid, z is

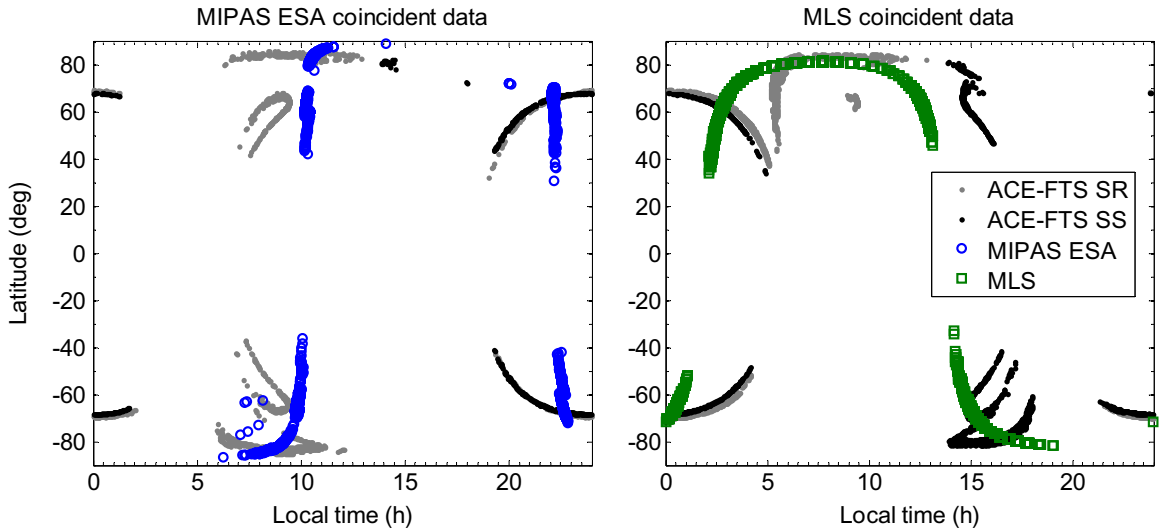


Fig. 1. Local time vs latitude of ACE-FTS H₂O retrievals (Sunrise: gray dots; Sunset: black dots) coincident within 3 h and 350 km with those of (left) MIPAS ESA and (right) MLS.

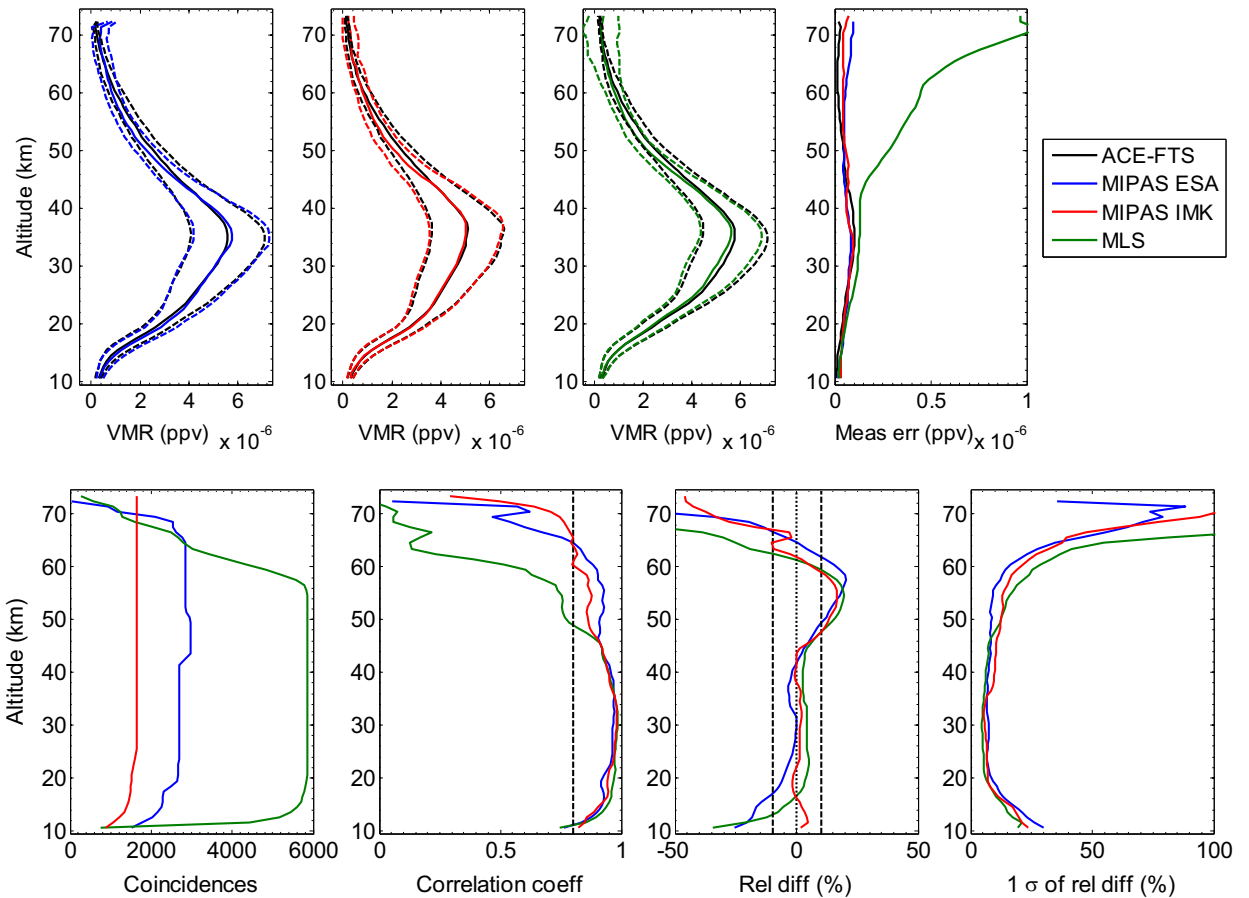


Fig. 2. Results for O₃ comparisons using coincidence criteria of within 3 h and 350 km. The first three top panels show the mean coincident VMR profiles (solid lines) $\pm 1\sigma$ variation (dashed lines), and the top right panel shows the measurement error for each instrument. The bottom panel shows, from left to right, the number of coincident profiles, the correlation coefficients, the mean of the relative differences (ACE-FTS minus other instrument) in percent, and the standard deviations of the relative differences in percent.

altitude, and $G(h, z)$ is the normalized Gaussian distribution,

$$G(h, z) = \frac{2\sqrt{2\ln 2}}{FWHM(h)\sqrt{2\pi}} \exp\left(-\frac{1}{2} \frac{(z-h)^2}{(FWHM(h)/2\sqrt{2\ln 2})^2}\right), \quad (2)$$

where $FWHM(h)$ (the full-width half-maximum) is the square root of the difference between the squared vertical resolution of the profile with coarser resolution, X_c , and the squared vertical resolution of X_f at altitude level h . Since ACE-FTS has a 3–4 km vertical resolution, the MIPAS and MLS VMR profiles were smoothed only in altitude regions where their vertical resolution was finer than 3 km, and ACE-FTS profiles were smoothed only in altitude regions where the coincident profile's vertical resolution was coarser than 4 km. Neither profile was smoothed in regions where the vertical resolutions were both between 3 and 4 km.

To assess the quality of the ACE-FTS VMR profiles, the comparisons consist of the calculation of three main metrics: the correlation coefficients, mean relative differences, and standard deviations of relative differences at each altitude. For all comparisons, calculated differences are with respect to ACE-FTS. The altitude dependent correlation coefficient, r , was calculated in the usual way,

$$r = \frac{1}{n-1} \sum_i^n \left(\frac{X_i - \bar{X}}{\sigma_X} \right) \left(\frac{Y_i - \bar{Y}}{\sigma_Y} \right), \quad (3)$$

where n is the number of collocated measurements, X represents the ACE-FTS data with a mean value of \bar{X} , Y represents the data from the correlative data set with a mean value of \bar{Y} , and σ is the standard deviation.

The ACE-FTS, MIPAS, and MLS retrievals all allow for negative concentrations (with the exception of MIPAS IMK-IAA CO and H₂O), and the negative VMR values have been left in the analysis as to not skew the means. When calculating percent differences, negative values can cause spuriously large results due to the average of two compared values being close to zero. Therefore, instead of calculating mean percent differences, at each altitude the mean of the relative differences was calculated as the mean of the absolute differences (relative to ACE-FTS) divided by the mean of both the combined ACE-FTS and correlative data set values,

$$rel\ diff = 2n \frac{\sum_i^n X_i - Y_i}{\sum_i^n X_i + Y_i} \times 100\%. \quad (4)$$

Similarly, the standard deviations of the relative differences were calculated at each height as the standard deviations of the absolute differences divided by the mean of the combined ACE-FTS and coincident data set.

4. Results

In the comparison results of the following sections, when “standard deviation” is used, it refers to the standard deviation of the relative differences (not the standard deviation of the measurement data). The standard deviation of the measurement data will be referred to as the

“measurement variation”. In all figures, unless otherwise indicated, ACE-FTS plots are in black, MIPAS ESA plots are in blue, MIPAS IMK-IAA are in red, and MLS plots are in green. The term “measurement error” is used to describe the reported error for each instrument. For ACE-FTS the measurement error represents the statistical fitting error, for MLS it is the estimated retrieval precision, and for both MIPAS ESA and MIPAS IMK-IAA it is the noise error standard deviation (note that none of these is an estimate of total retrieval error).

4.1. Comparisons of O₃

The mean coincident O₃ profiles and corresponding measurement error are shown in the top panel of Fig. 2, with dashed lines indicating the 1- σ measurement variation, and the comparison results are shown in the bottom panel of Fig. 2.

The best results can be seen around the O₃ peak. Between 20 and 45 km, the mean relative differences are all typically within $\pm 5\%$. ACE-FTS exhibits a positive bias with respect to MLS, on the order of 4% throughout the region, and a slight negative bias with respect to MIPAS ESA, on the order of -2% ; in this region the MIPAS IMK-IAA relative differences are between those for MIPAS ESA and MLS. In this altitude region, the correlation coefficients and the standard deviations of the relative differences for comparisons with all three data sets are quite similar. The correlation coefficients are all above 0.9 and all standard deviations are between 4 and 10%.

In the USLM, ACE-FTS exhibits a pronounced positive bias with respect to all three data sets. It is possible that this bias is in part due to diurnal variation in O₃ along the ACE-FTS line of sight, which is not accounted for in the forward model and is known to be an issue for occultation limb sounders. The ACE-FTS positive bias reaches a maximum of $\sim 18\%$ near 56 km, with MIPAS ESA standard deviations on the order of 10%, those of MIPAS IMK-IAA near 15%, and those of MLS near 18%. At the upper altitudes, correlation coefficients and standard deviations get worse with increasing altitude. For all three data sets, the standard deviations are typically greater than 50% above ~ 65 km. The correlation coefficients for both MIPAS data sets are typically greater than 0.5 at all altitudes and are greater than 0.8 at altitudes below 64 km and 60 km for MIPAS ESA and MIPAS IMK-IAA, respectively. The MLS correlation coefficients are greater than 0.5 at altitudes below 60 km and are greater than 0.8 at altitudes below 49 km. Above ~ 60 km, ACE-FTS exhibits a negative bias with respect to all three data sets. The bias becomes more negative with increasing altitude, with a negative bias beyond -75% with respect to all three data sets at the highest altitude level.

ACE-FTS also tends to exhibit a negative bias with respect to all three instruments below 20 km that gets more negative with decreasing altitude. In this region correlation coefficients are typically greater than 0.75, and at the lowest altitude level the negative biases range from -12% (MIPAS IMK-IAA) to -34% (MLS), with standard deviations on the order of 25%.

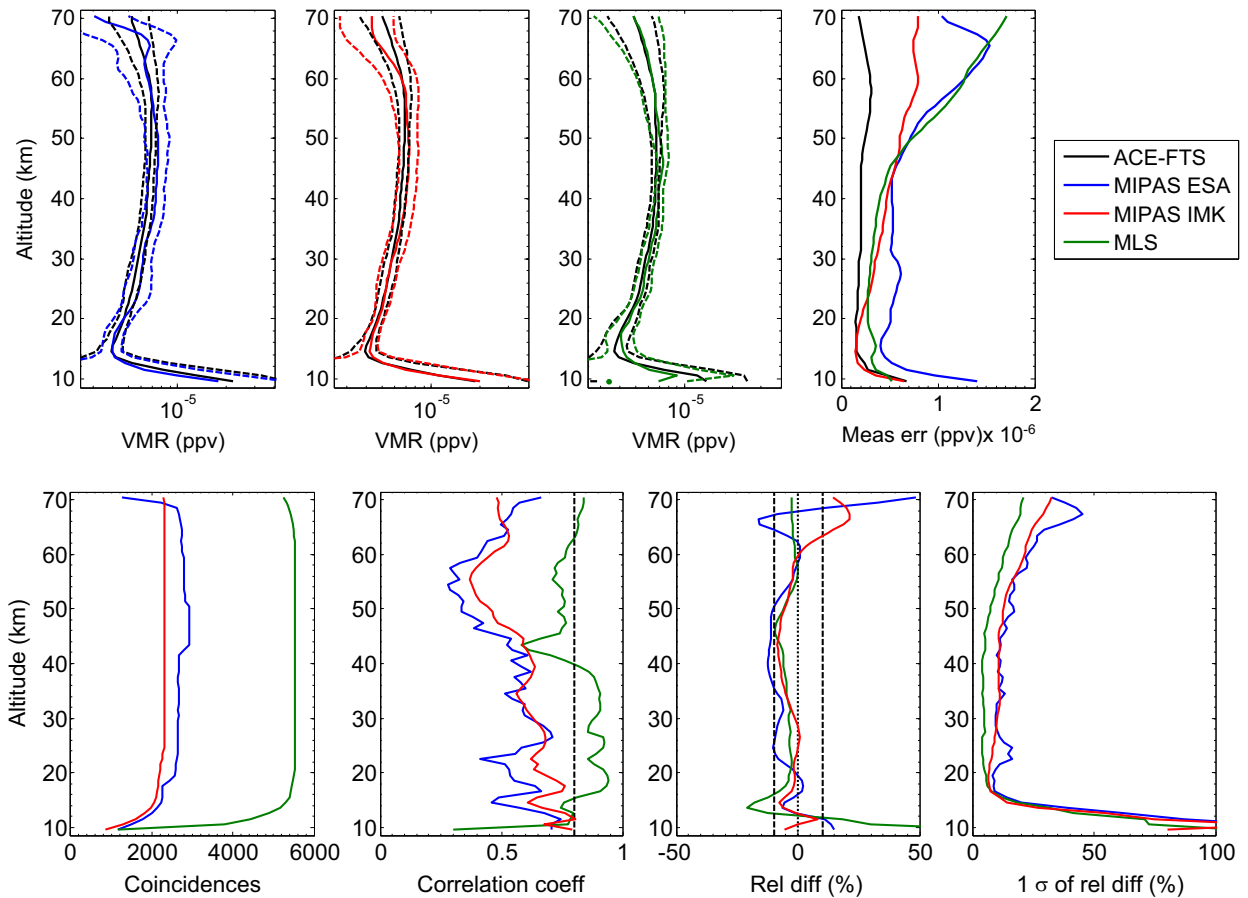


Fig. 3. Same as Fig. 2, but for H₂O. Note that for the top panel the VMR values are plotted on a logarithmic scale, while the measurement error is plotted on a linear scale.

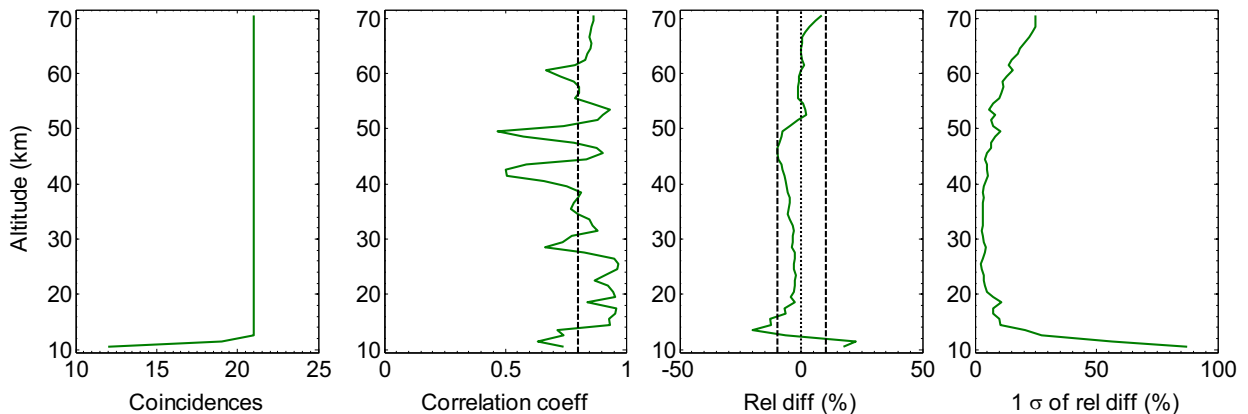


Fig. 4. Results for ACE-FTS and MLS H₂O comparisons using coincidence criteria of within 15 min and 25 km. The panel shows, from left to right, the number of coincident profiles, the correlation coefficients, the mean relative differences (ACE-FTS minus other instrument) in percent, and the standard deviations of the relative differences in percent.

4.2. Comparisons of H₂O

The top panel of Fig. 3 shows the mean coincident H₂O profiles, and the corresponding measurement error, with dashed lines indicating the 1-σ measurement variation, and the comparison results are shown in the bottom panel of Fig. 3.

At nearly all altitude levels, the MLS comparisons yielded better correlation and better standard deviations than either of the MIPAS data sets. Both the MIPAS ESA and IMK-IAA data sets exhibit greater measurement variation than ACE-FTS data, and the MIPAS ESA profiles are prone to large spikes and oscillations in VMR throughout the stratosphere and lower mesosphere. This is primarily due

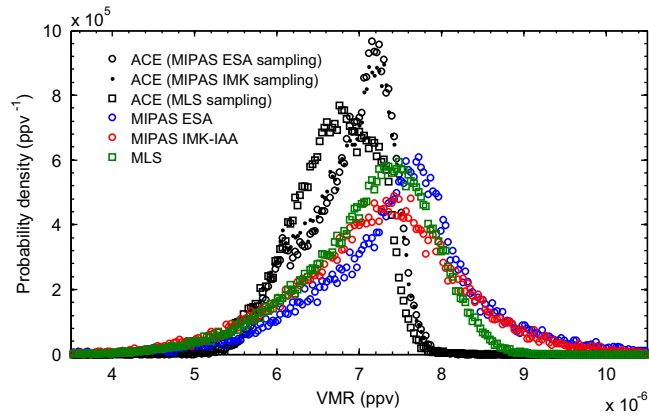


Fig. 5. H₂O VMR probability distribution functions for all coincident data sets (within 3 h and 350 km of ACE-FTS) in the 45–55 km altitude region. Black circles represent the ACE-FTS data coincident with MIPAS ESA, black dots represent the ACE-FTS data coincident with MIPAS IMK-IAA, black squares represent the ACE-FTS data coincident with MLS, blue circles represent the coincident MIPAS ESA data, red circles represent the coincident MIPAS IMK-IAA data, and green squares represent the coincident MLS data. (For interpretation of the references to color in this figure legend, the reader is referred to the web version of this article.)

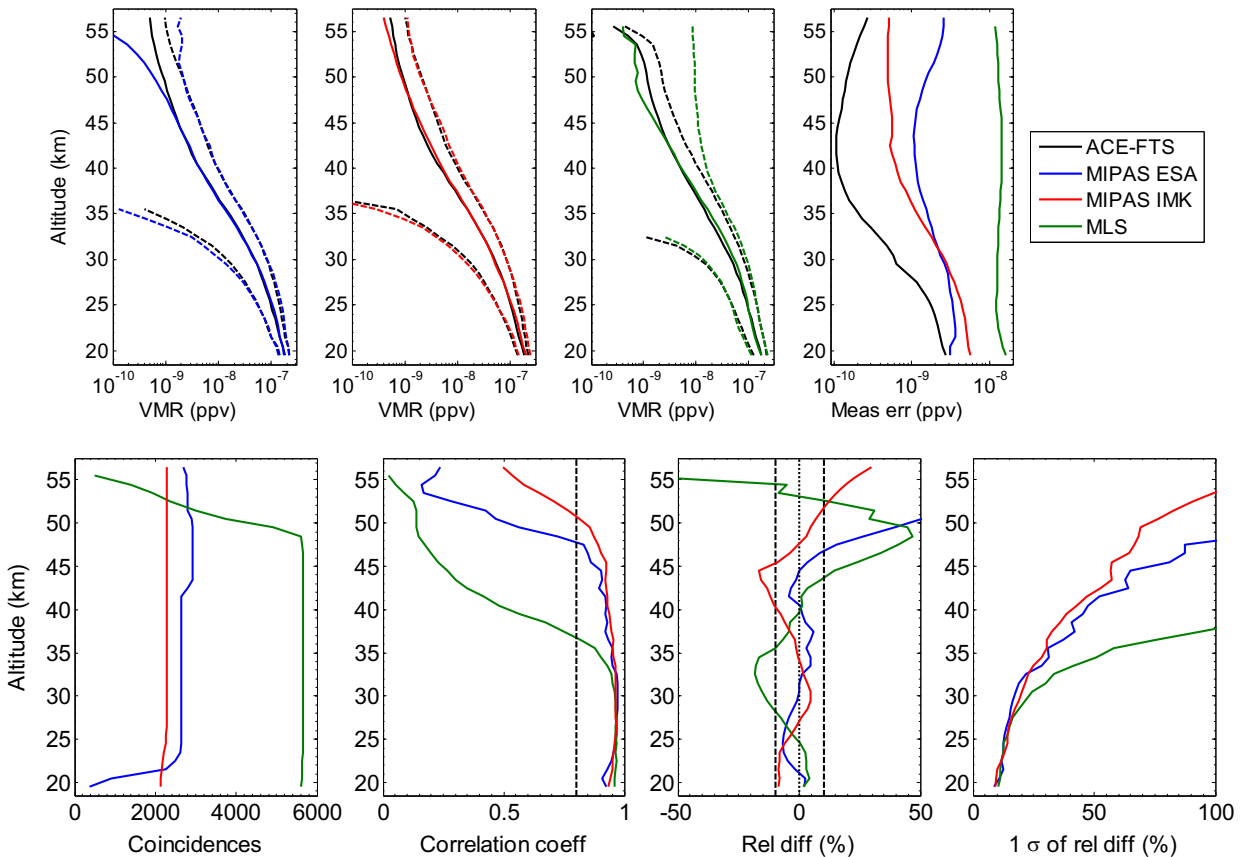


Fig. 6. Same as Fig. 2, but for N₂O.

to the fact that the a posteriori regularization is not applied for the MIPAS ESA H₂O retrievals. As such, the MIPAS ESA comparisons yielded the lowest correlation coefficient values and greatest standard deviations, and the comparisons exhibit more oscillations.

Just below the observed hygropause (~ 15 km), where the H₂O VMR increases exponentially with decreasing

altitude, ACE-FTS exhibits a negative bias with respect to all three data sets. The negative bias with respect to MIPAS ESA, MIPAS IMK-IAA, and MLS is at its most negative near 13 km at -7% , -8% and -21% , respectively, with standard deviations increase significantly with decreasing altitude, due to increasing water vapour variability, up to $\sim 115\%$ at the

lowest altitude level. In order to determine if the negative bias truly represents the ACE-FTS data, and is not simply an artifact of the large H₂O variability in the region, a comparison with MLS data was made using coincidence criteria of within 15 min and within 25 km. The results, shown in Fig. 4, show that, with 21 coincident profiles, ACE-FTS still exhibits a negative bias of −20% at 13 km, with a standard deviation of the relative differences value of 21%.

From just above the observed hygropause up to the lower mesosphere, ACE-FTS exhibits a consistent negative bias with respect to both the MIPAS and the MLS data sets, as seen in Fig. 3. Between 16 and 61 km, mean relative differences range from −12 to +2%. The MLS standard deviations range between 4 and 14%, and the MLS correlation coefficients are on the order of 0.85 in the mid-stratosphere and 0.75 in the upper stratosphere and mesosphere. The MIPAS ESA and IMK-IAA comparisons yielded similar standard deviations and similar correlation coefficients to one another. The correlation coefficients tend to decrease with altitude from ~0.55 and ~0.65, respectively, in the stratosphere to ~0.35 and ~0.45 in the USLM; near the hygropause, the standard deviations are on the order of 9%, and increase to ~22% near 60 km.

The correlation coefficient profiles for all three data sets exhibit a local minimum in the USLM. This appears to be

due to a significant difference in the ACE-FTS H₂O VMR distribution in this region with those of the other data sets. Fig. 5 shows the probability distribution functions for all coincident data in the 45–55 km region.

One feature they all have in common is that the distributions are more skewed to lower VMR values, with all four data sets exhibiting minimum VMR values in the 4–5 ppmv range. However, the ACE-FTS data in all comparisons appear to have a much sharper “cut-off” at the higher end of the distributions. The MIPAS and MLS distributions show a much broader range of VMR values around their respective peak values, and all show maximum values in the range of 9–12 ppmv, whereas the ACE-FTS tends not to exhibit any H₂O VMR values above 8 ppmv. There are currently no known issues in the ACE-FTS H₂O retrieval that would constrain the VMRs to lower values.

4.3. Comparisons of N₂O

The mean coincident N₂O profiles, and corresponding measurement error, are shown in the top panel of Fig. 6, with dashed lines indicating the 1-σ measurement variation, and the comparison results are shown in the bottom panel of Fig. 6.

Between 19 and 34 km, all correlation coefficients are greater than 0.9, both the MIPAS ESA and IMK-IAA standard deviations increase from ~9% to ~28% with

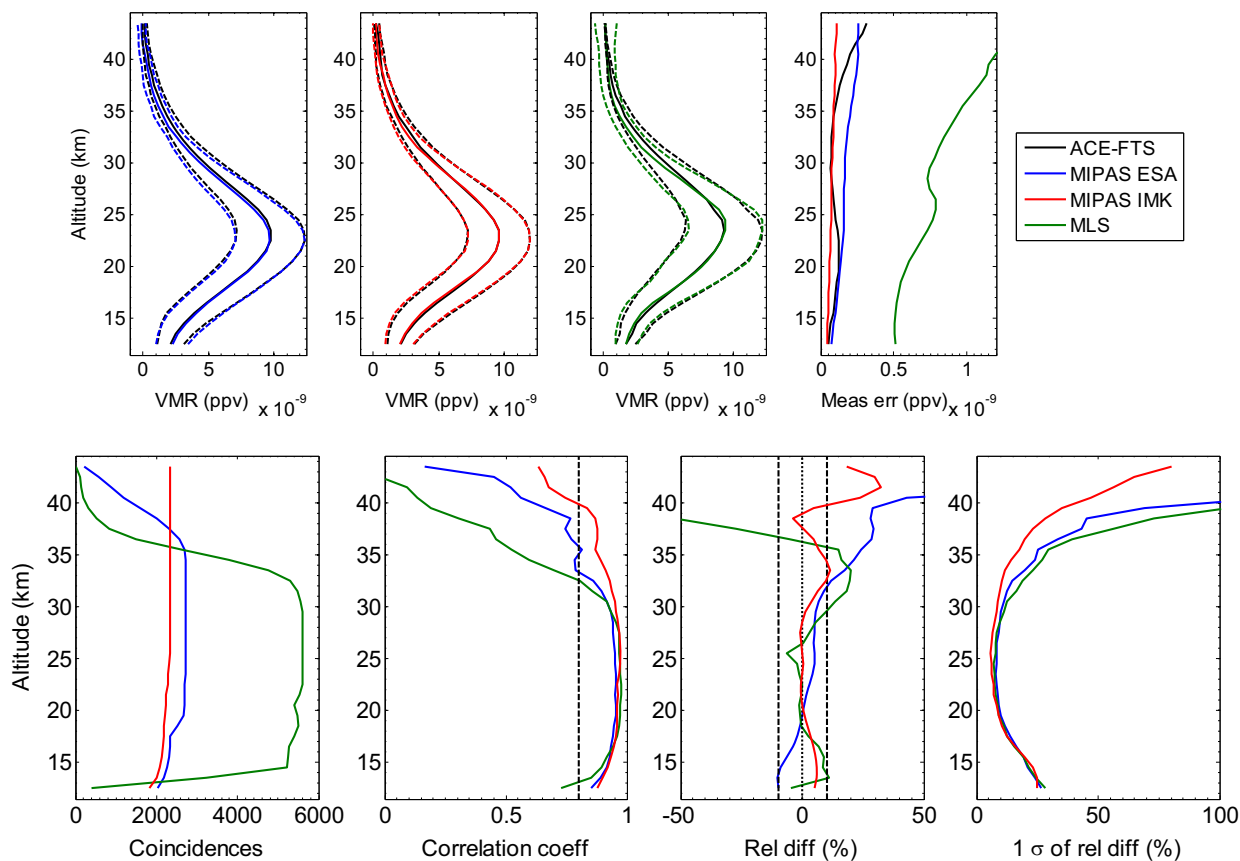


Fig. 7. Same as Fig. 2, but for HNO₃.

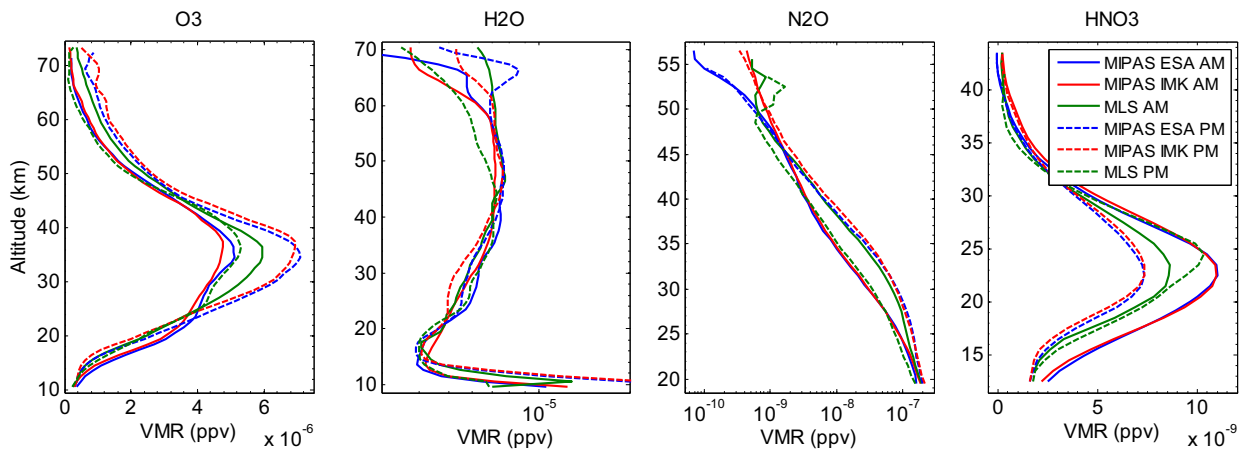


Fig. 8. Mean local morning (AM; solid lines) and local evening (PM; dashed lines) VMR profiles for MIPAS ESA, MIPAS IMK-IAA, and MLS data coincident with ACE-FTS within 3 h and 350 km. Plots from left to right are for O_3 , H_2O , N_2O , and HNO_3 .

increasing altitude, and the MLS standard deviations increase from 11% to 45%. The MIPAS mean relative differences range from -9 to $+5\%$, and the MLS values change from $\sim +4\%$ to -18% with increasing altitude.

Above 34 km, the MLS comparisons yield poorer results due to the large measurement variation in the MLS data at the upper altitudes. The standard deviations are greater than 50% at 35 km and above, greater than 100% above 37 km, and the correlation coefficients are less than 0.5 above 40 km.

The MIPAS ESA correlation coefficients are greater than 0.8 up to 48 km, however the standard deviations increase fairly linearly to 101% at this altitude. Between 34 and 48 km, the MIPAS ESA mean relative differences are within $\pm 6\%$. At higher altitudes, correlations and standard deviations worsen significantly (correlation near 0.2 and standard deviation well above 200%).

The MIPAS IMK-IAA correlation stays above 0.5 at all altitudes below 56 km, and the standard deviations are greater than 100% above 53 km. Between 34 and 53 km, ACE-FTS and MIPAS IMK-IAA typically agree within $\pm 16\%$.

4.4. Comparisons of HNO_3

The top panel of Fig. 7 shows the mean coincident HNO_3 profiles, and the corresponding measurement error, with dashed lines indicating the $1-\sigma$ measurement variation, and the comparison results are shown in the bottom panel of Fig. 7.

At and around the HNO_3 peak, ~ 18 to 31 km, comparison results for both MIPAS data sets and for MLS are all fairly similar. In this region, all correlation coefficients are above 0.9 and standard deviations are in the range of 6–12%. The MIPAS mean relative differences range from -1 to $+8\%$, whereas the MLS differences are in the range of -6 to $+16\%$.

In the 30–35 km region, ACE-FTS exhibits a positive bias of $\sim 20\%$ with respect to MLS, and above this region ACE-FTS and MLS exhibit weak to no correlation, and the standard deviations are greater than 100% above 39 km.

Towards 40 km, the MIPAS ESA correlation decreases to 0.62 and the standard deviation increases to 96%, and the mean relative difference increases to 36%. In the middle to upper stratosphere, the MIPAS IMK-IAA comparisons yield the best results, with correlation coefficients typically better than 0.63, standard deviations less than 80%, and mean relative differences ranging from 0–32%.

Below 18 km, all correlation coefficients are typically above 0.75, the standard deviations increase to $\sim 17\%$ at the lowest altitude level, and the mean relative differences are all within $\pm 11\%$.

4.5. Diurnal biases in O_3 , H_2O , N_2O and HNO_3

In order to determine any possible diurnal biases in the ACE-FTS data sets, comparisons were made between ACE-FTS and the three other data sets, separating the data into local morning (AM) and local evening (PM) data. Although there are many intricacies that arise when determining diurnal differences when comparing solar occultation measurements with emission measurements, the focus of this study is to identify critical regions where there are significant diurnal differences. The mean AM and PM VMR profiles for the MIPAS and MLS data sets are shown in Fig. 8. It can be seen that, in most regions, MLS AM data is more similar to the MIPAS PM data than to the MIPAS AM data. This is due to the MIPAS AM and the MLS PM observations typically being made during sunlit hours, and MIPAS PM/MLS AM observations typically being made in darkness. In the O_3 , H_2O , N_2O , and HNO_3 comparisons with all three correlative data sets, a clear systematic difference between AM and PM results is observed. As seen in the top panel of Fig. 9, for all four species, at nearly all altitude levels, comparisons with both MIPAS data sets yield larger standard deviations in the AM comparisons than those for the PM, and the MLS comparisons yield larger standard deviations in the PM.

Typically, the standard deviation profiles are strongly correlated with the mean reported percent measurement error profiles of the individual data sets, which are shown

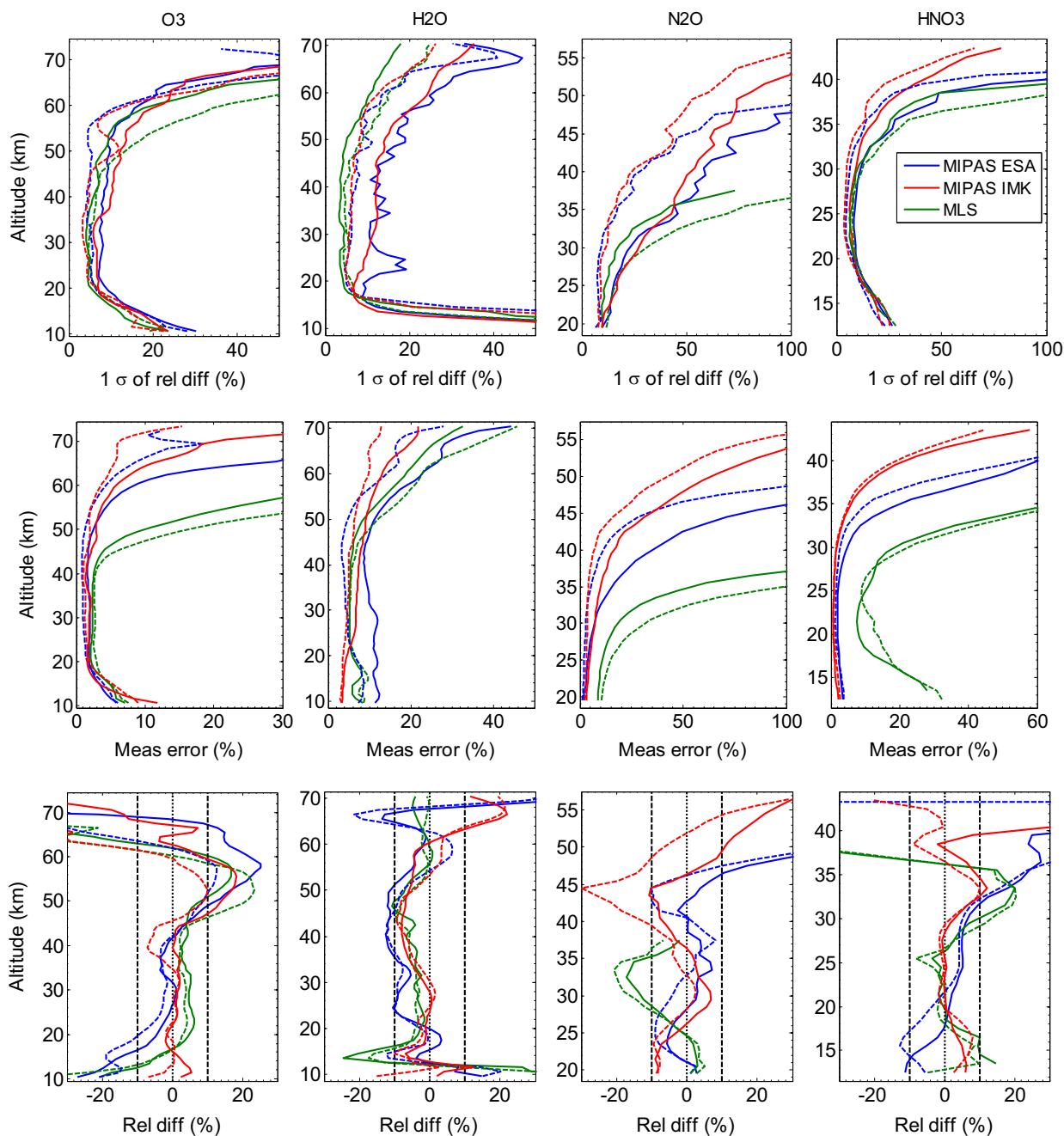


Fig. 9. Results for local morning (AM; solid lines) and local evening (PM; dashed lines) comparisons using coincidence criteria of within 3 h and 350 km. Plots from left to right are for O₃, H₂O, N₂O, and HNO₃. The top panel shows standard deviations of the relative differences, the middle panel shows mean percent measurement errors, and the bottom panel shows mean relative differences (ACE-FTS minus other instrument) in percent.

in the middle panel of Fig. 9. The mean MIPAS error for all four species (both ESA and IMK-IAA) tends to be greater for AM retrievals than for evening retrievals, whereas the mean MLS error tends to be greater for PM retrievals.

The only significant exception to these diurnal biases is for the H₂O results at and below the hygropause. Despite the fact that in this region the MIPAS (both ESA and IMK-IAA) measurement errors remain greater for AM comparisons and the MLS errors remain greater for PM

comparisons, the opposite is true for the standard deviations—the MIPAS standard deviations are greater in the PM and those for the MLS comparisons are greater in the AM.

The bottom panel of Fig. 9 shows the mean relative differences between ACE-FTS and the three different data sets for both AM and PM comparisons. In the middle stratosphere, there is a clear diurnal bias in the O₃ relative differences. The ACE-FTS bias is typically more positive for AM comparisons than for PM comparisons, by up to 7%.

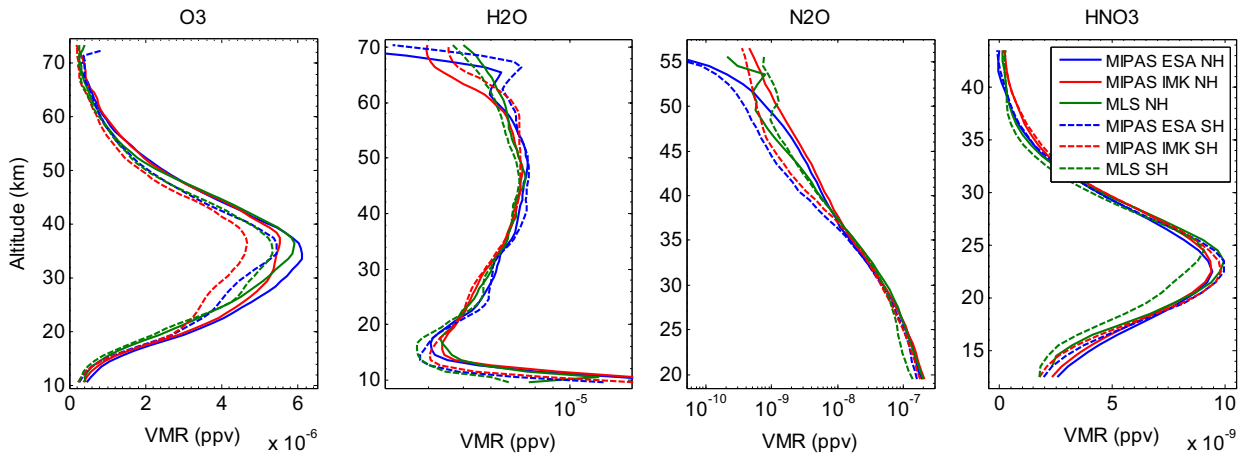


Fig. 10. Mean Northern hemisphere (NH; solid lines) and Southern hemisphere (SH; dashed lines) VMR profiles for MIPAS ESA, MIPAS IMK-IAA, and MLS data coincident with ACE-FTS within 3 h and 350 km. Plots from left to right are for O_3 , H_2O , N_2O , and HNO_3 .

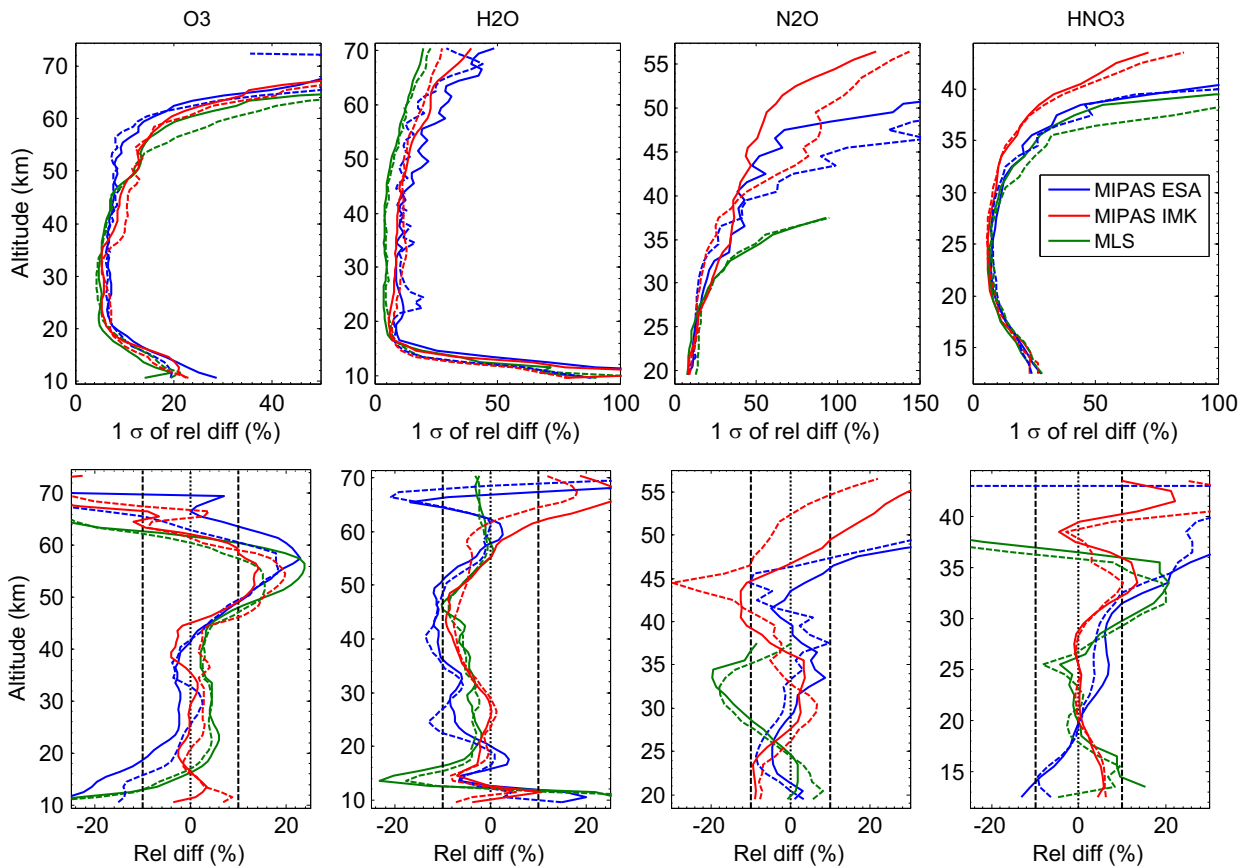


Fig. 11. Results for NH (solid lines) and SH (dashed lines) comparisons using coincidence criteria of within 3 h and 350 km. Plots from left to right are for O_3 , H_2O , N_2O , and HNO_3 . The top panel shows the standard deviations of the relative differences, and the bottom panel shows the mean relative differences (ACE-FTS minus other instrument) in percent.

Between 20 and 45 km, the average PM ACE-FTS bias, over all comparisons, is -0.3% , whereas the average AM bias is 1.6% .

The ACE-FTS O_3 positive bias in the stratopause region does not exhibit a consistent diurnal difference between the MLS and MIPAS comparisons, and therefore it is not possible

to conclude whether there is an ACE-FTS diurnal bias or not. In the MIPAS comparisons, the AM ACE-FTS positive bias is on the order of 20% and is reduced to $\sim 10\%$ in the PM comparisons; in the MLS comparisons the AM ACE-FTS positive bias reaches a maximum of 17% and the PM maximum reaches 23%. These differences due to local time

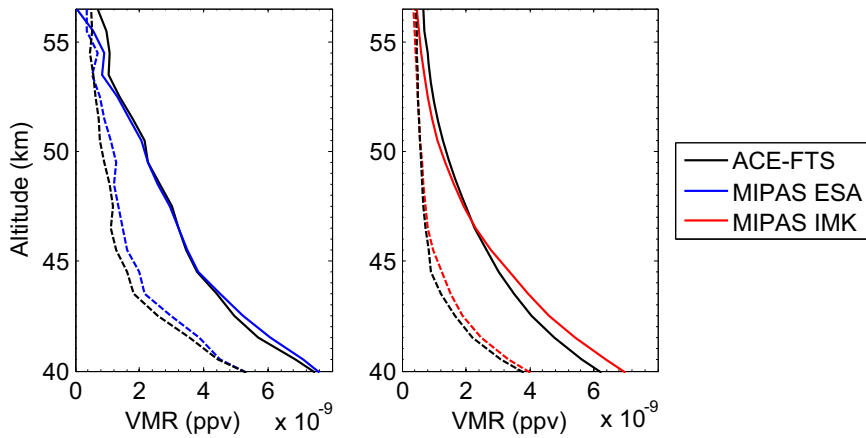


Fig. 12. Mean coincident ACE-FTS and MIPAS ESA and IMK-IAA N₂O VMR profiles in the upper stratosphere for data in the NH (solid lines) and the SH (dashed lines).

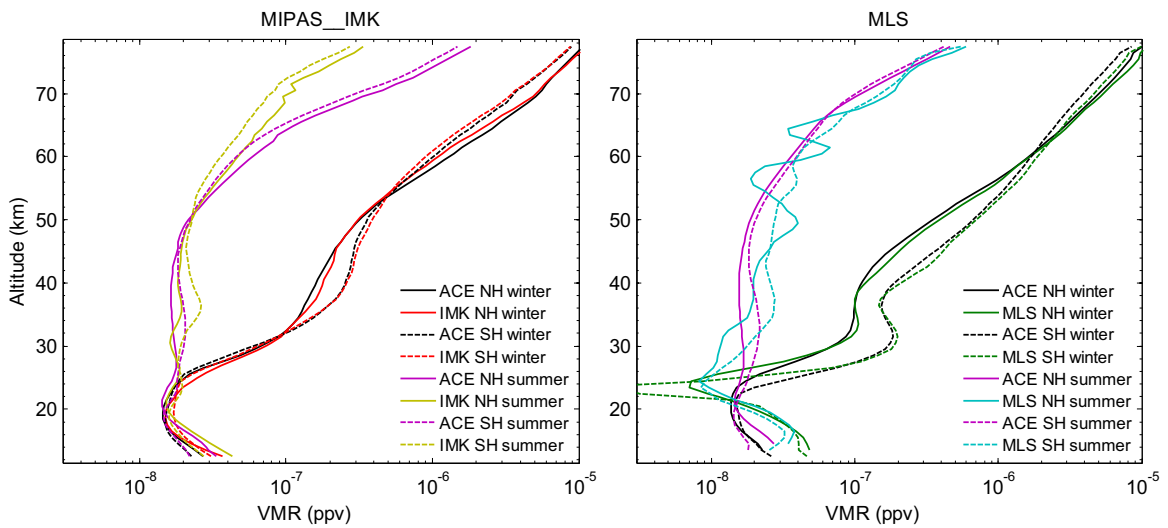


Fig. 13. Mean coincident CO profiles for comparisons in the winter and summer months for both NH and SH (December–February for NH winter and SH summer, June–August for NH summer and SH winter).

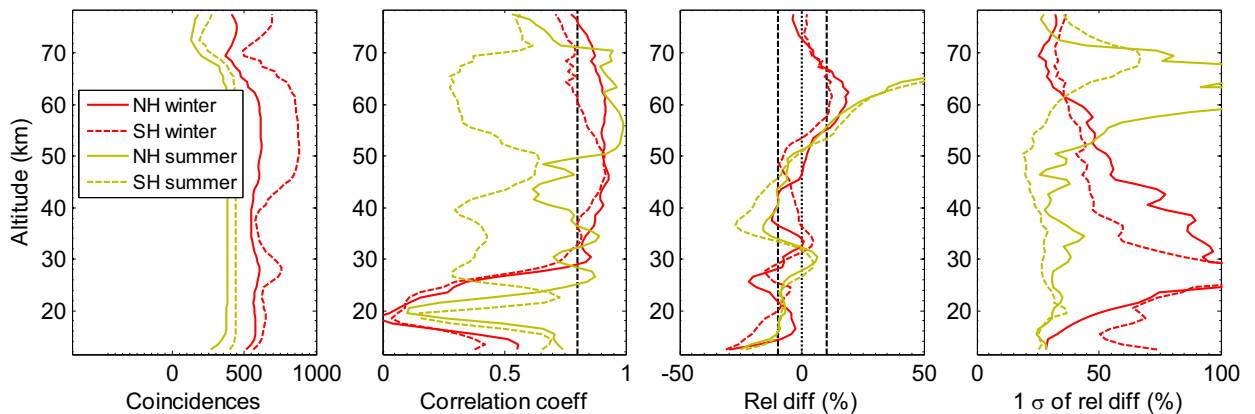


Fig. 14. Results for MIPAS IMK-IAA CO comparisons using coincidence criteria of within 3 h and 350 km. From left to right, the panels show the number of coincident profiles, the correlation coefficients, the mean relative differences (ACE-FTS minus MIPAS) in percent, and the standard deviations of the relative differences in percent. Solid lines represent NH comparisons, dashed lines represent SH comparisons, red lines represent winter comparisons, and yellow lines represent summer comparisons. (For interpretation of the references to color in this figure legend, the reader is referred to the web version of this article.)

further indicate that at least some portion of the ACE-FTS positive bias is likely due to diurnal variations along the line of sight. Above ~ 50 km, it is likely that the ACE-FTS positive bias with respect to MIPAS is larger for AM measurements in part because the ACE-FTS measurements are predominantly sunrise measurements, just as O_3 concentrations are beginning to rapidly decrease due to photolysis, whereas the MIPAS observations are made after this rapid decrease.

For H_2O , there is no consistent systematic difference between AM and PM comparison mean relative differences. Between 16 and 52 km, for comparisons with all three data sets, the AM and PM relative differences differ by less than $\pm 5\%$. Outside of this altitude region, AM and PM relative difference results differ by up to 21%.

For N_2O , with the exception of MLS comparisons below 26 km, all three data sets tend to exhibit more positive mean relative differences for the AM comparisons than for PM comparisons, by on average 7%. Above 35 km, where the MLS results do not agree with ACE-FTS, the difference between the AM and PM MIPAS relative differences is typically $\sim 10\%$ (where the data sets agree well with ACE-FTS). Below 26 km, the MLS AM mean relative differences are ~ 1 to 2% lower than those for the PM comparisons, which are considered significant as the standard errors in this region are on the order of 0.3%.

There is no consistent systematic difference between AM and PM comparison mean relative differences for HNO_3 . Below 38 km the difference between the AM and PM MLS relative differences is within $\pm 5\%$, and within $\pm 5\%$ for the MIPAS IMK-IAA comparisons below 35 km. Between 14 and 35 km the MIPAS ESA relative differences are systematically more positive for AM comparisons than for PM comparisons by up to 10% near 17 km, but only by 1–2% closer to the HNO_3 peak.

4.6. Hemispheric biases in O_3 , H_2O , N_2O and HNO_3

The mean Northern hemisphere (NH) and Southern hemisphere (SH) VMR profiles for the MIPAS and MLS data sets are shown in Fig. 10, and the differences between the NH comparison results and those of the SH, shown in Fig. 11, are less pronounced than those between AM and PM results.

For O_3 , between 12 and 51 km, the difference between NH and SH MLS relative differences is typically within $\pm 2\%$, with standard errors on the order of 0.2%. In the middle stratosphere the NH MIPAS (both ESA and IMK-IAA) relative differences tend to be more negative, by ~ 2 to 6%. Between 35 and 55 km, the NH MIPAS IMK-IAA relative differences are $\sim 6\%$ lower, whereas there is

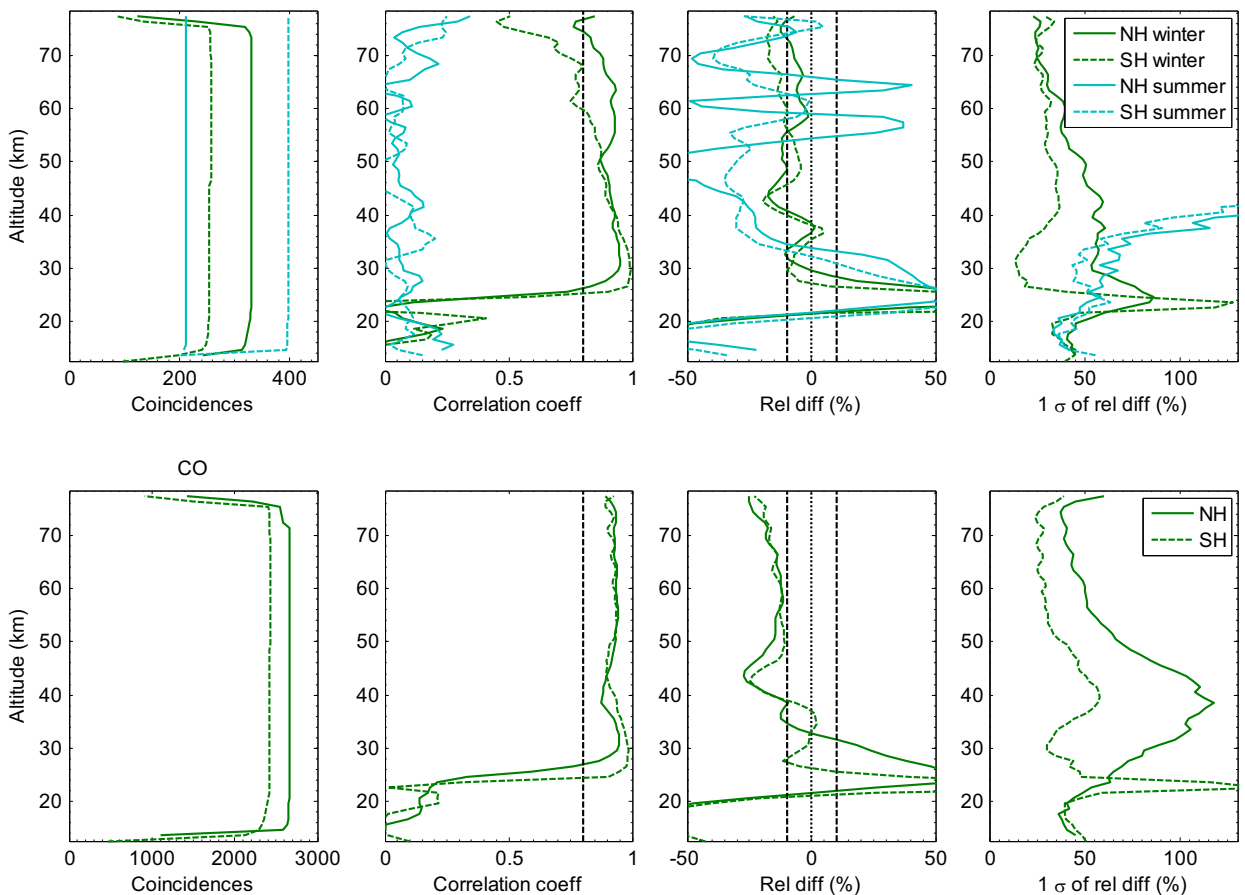


Fig. 15. Results for MLS CO comparisons using coincidence criteria of within 3 h and 350 km. In the top panel solid lines represent winter comparisons and dashed lines represent summer comparisons. The bottom panel shows comparisons for all NH data (solid lines) and SH data (dashed lines) where the summer months (June–August for NH, December–January for SH) have been excluded.

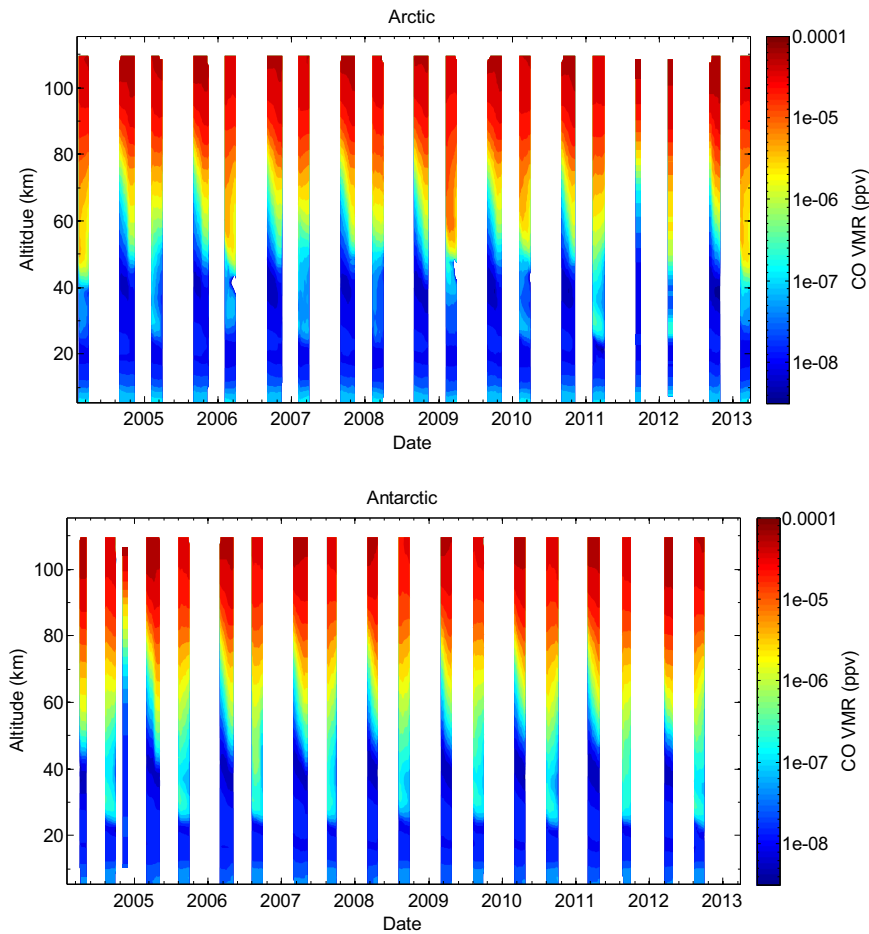


Fig. 16. ACE-FTS CO profile time series for (top) 70–90°N and (bottom) 70–90°S. Daily profiles represent the 30-day mean.

essentially no hemispheric difference (within $\pm 1\%$) for the MIPAS ESA results.

For H_2O , throughout the atmosphere, the differences between NH and SH relative differences are typically within $\pm 4\%$ for comparisons with all three data sets. The hemispheric differences tend to increase at the altitude extremes, reaching up to a maximum difference of 33% (standard errors on the order of 1%) near the upper altitude limit and 27% (standard errors of $\sim 6\%$) at the lower limit.

For N_2O , below 38 km, the differences between NH and SH relative differences are typically within $\pm 8\%$ for comparisons with all three data sets. In the upper stratosphere (where the MLS comparison results do not agree with ACE-FTS) there does appear to be a significant difference between the MIPAS (both ESA and IMK-IAA) NH and SH comparisons. The MIPAS standard deviations for NH comparisons are better, by $\sim 35\%$ for IMK-IAA and $\sim 70\%$ for ESA, than for those in the SH, with a similar hemispheric difference in measurement error. The better standard deviations in the NH upper stratosphere are mostly due to the fact that mean N_2O concentrations, shown in Fig. 12, are ~ 20 to 65% greater in the NH than in the SH in this region—leading to greater N_2O signal-to-noise ratio for measurements in the NH, as well as larger reference

values when calculating the standard deviations. The greater concentrations in the NH upper stratosphere is mostly due to greater descent of N_2O -rich air in the winter months, especially during stratospheric warming events, as discussed by [23]. Above 40 km, the MIPAS NH relative differences tend to be 5–15% more positive than in the SH, indicating that ACE-FTS N_2O exhibits a systematic positive bias with respect to MIPAS data in the NH stratopause region.

For HNO_3 , below 35 km, the differences between NH and SH relative differences are typically within $\pm 5\%$ for comparisons with all three data sets. The absolute hemispheric differences are less than 20% up to 40 km; and in this region and above, where only the MIPAS IMK-IAA data compare well with ACE-FTS, MIPAS IMK-IAA SH data are up to 18% greater than NH data.

4.7. Comparisons of CO

Since CO in the middle stratosphere and above has a strong seasonal cycle, the MIPAS and MLS data were separated into summer and winter bins prior to comparing with ACE-FTS. For NH, summer/winter was considered to be June–August/December–February, and vice versa in the SH. As the lifetime of atmospheric CO in this region is on the order of a

Table 2

Average ACE-FTS systematic biases for O₃, H₂O, N₂O, and HNO₃ comparisons using coincidence criteria of within 3 h and 350 km. Values represent altitude regions where correlation coefficients are better than 0.5 and standard deviations of the relative differences are better than 50%.

Species	Altitude range (km)	Mean bias (%)
O ₃	10–45	+2
	46–60	0 to +19
H ₂ O	13–16	–10
	17–46	–2 to –10
	47–70	±8
N ₂ O	20–35	–3
	MIPAS: 36–44	–8
HNO ₃	13–17	+7
	18–27	±2
	28–38	+3 to +19

week to months, the data were not separated by local time. Fig. 13 shows the mean winter and summer CO profiles in both the NH and SH. As expected the concentrations in the mid-stratosphere to upper mesosphere are greater in the winter, when there is downward descent in the high latitudes, than during the summer.

4.7.1. MIPAS IMK-IAA

As seen in Fig. 14, the ACE-FTS and MIPAS relative differences for all four regions are fairly consistent below 60 km. In both hemispheres, the ACE-FTS data tend to exhibit a negative bias.

In the lower stratosphere the negative bias ranges from –2 to –31%. Higher up, near 27 km, the negative bias reaches –22% in the winter NH and –15% in the winter SH (with only moderate correlation and standard deviations greater than 100%), and the negative bias reaches –27% in the summer SH and –16% in the summer NH. Below 51 km, the winter ACE-FTS negative bias with respect to MIPAS is on average –8%, and is –9% in the summer. In the 53–72 km region, winter ACE-FTS data tends to exhibit a positive bias on the order of 0–18%, whereas the summer relative differences are much larger, increase to values greater than 100% above 66 km.

With the exception of winter SH data, at the lowest altitudes, near 15 km, ACE-FTS and MIPAS data exhibit moderate correlation and standard deviations on the order of 28%; both correlation coefficients and standard deviations tend to degrade with altitude, approaching the CO VMR minimum (~1.5 ppbv near 20 km). Around 25–28 km, there is a large increase in the winter standard deviations, up to 135%, and there is only low to moderate correlation between the two data sets. This is due to the fact that the ACE-FTS CO VMR often exhibits large negative spikes in this region, and this is also the region where the winter MIPAS IMK-IAA CO measurement error peaks (percent error of ~46% at 27 km). Above 28 km, the winter correlation coefficients are greater than 0.7, with slightly stronger correlation exhibited in the NH than SH; the summer NH correlation coefficients are above 0.6; and in the summer SH there is only moderate correlation. In this region, the winter standard deviations tend to decrease with altitude from ~100% to ~34% at the highest altitude

levels. The summer standard deviations are typically on the order of 25–40%, except in the middle mesosphere where they increase up to 155% near 62 km in the NH and 67% near 70 km in the SH.

4.7.2. MLS

As seen in the top panel of Fig. 15, the winter MLS data compares relatively well with ACE-FTS above 25 km. In this region the correlation coefficients are typically greater than 0.7, and standard deviations decrease with altitude from ~60 to 80% in the middle stratosphere to ~30% in the mesosphere. In the 29–42 km region, ACE-FTS winter CO concentrations are typically less than those of MLS with relative differences between –21 and 5%, and above 40 km winter ACE-FTS data exhibits a negative bias between –1 and –21%, with an average value of –8%. Between 22 and 25 km, the winter MLS data in the high latitudes exhibits large negative VMR spikes. This leads to a sharp increase in relative differences and standard deviations, up to 172% and 127% respectively, and a sharp decrease in correlation, down to ~0 near 21 km from 0.9 at 25 km. The mean MLS CO VMRs in this region are much smaller than those of both ACE-FTS and MIPAS IMK-IAA, indicating that MLS is likely the source of the negative bias. Below this region, ACE-FTS and MLS are very poorly correlated and the mean profiles do not agree in shape or magnitude.

Due to low summer concentrations, and therefore a weaker CO signal in the MLS radiance observations, the MLS summer data does not agree well with ACE-FTS at most altitudes (top panel of Fig. 15). There is only weak correlation between the summer data sets in both the NH and SH. Standard deviations are on the order of 40% below 25 km, however the mean relative differences are on the order of ±65%, as the MLS data are relatively noisy in this region and occasionally are negative (~5% of the VMR values are negative). Summer standard deviations increase to greater than 100% at and above 40 km.

The bottom panel of Fig. 15 shows comparison results with all MLS in the NH and SH when the summer data have been excluded. Above 25 km, the standard deviations exhibit a clear hemispheric bias, with larger standard deviations in the NH than in the SH, especially near 30 km where the difference is on the order of 60%. This is because near 30 km the SH winter high latitudes exhibit much greater CO concentrations (by up to an order of magnitude) than in other regions at this altitude. This is due to wintertime descent into the SH polar vortex being more consistent than in the NH. As Fig. 16 shows, every winter in the high SH latitudes (poleward of 70°S), CO is consistently transported down from the upper atmosphere into the middle stratosphere.

However, in the NH high latitudes (poleward of 70°N), although there is typically some descent of CO-rich air into the winter middle stratosphere, it is rarely as great in magnitude as it is in the Antarctic winter. The one NH winter that most exhibits SH-like stratospheric CO concentrations is in 2011, when there was a strong Antarctic-like Arctic vortex [24]. Above 25 km, the correlation coefficients are typically greater than 0.9, and above 33 km both the NH and SH relative differences tend to be negative (relative to ACE-FTS)

with average NH and SH mean relative differences of -17% and -14% , respectively.

5. Summary

This study compared ACE-FTS O_3 , H_2O , N_2O , HNO_3 , and CO profiles to correlative satellite data sets from the MIPAS (both the ESA and IMK-IAA data sets) and MLS instruments. All comparisons used coincidence criteria of profiles being measured within 3 h and 350 km of each other. Table 2 summarizes the ACE-FTS biases for each species (except CO) in altitude regions where the comparison correlation coefficients were typically better than 0.5 and the standard deviations of the relative differences were typically better than 50%. As well, systematic differences between ACE-FTS and the other instruments were examined for different observed latitude regions (NH and SH) and for different observed local times (morning and evening).

Near the O_3 peak, comparisons with MIPAS and MLS yield correlation coefficients that are typically better than 0.95 and standard deviations that are on the order of 6%. Below 16 km, ACE-FTS tends to exhibit a negative bias in the range of 0 to -35% . In the middle to upper stratosphere, mean relative differences are typically within $\pm 5\%$, with ACE-FTS exhibiting a small positive bias of $\sim 2\%$ in comparison to MIPAS IMK-IAA and MLS. In this region, the mean relative differences tend to be more positive (relative to ACE-FTS), by $\sim 2\%$, when comparing local morning data than for local evening comparisons. ACE-FTS exhibits a positive bias in the USLM, which tends to peak within the stratopause region at ~ 10 to 25%, depending on latitude and local time. These results are slightly better than the results reported by [11].

At nearly all altitudes, the MLS H_2O comparisons yield better results, in terms of correlation coefficients and standard deviations, than the MIPAS H_2O comparisons. ACE-FTS and MLS exhibit strong correlation throughout the lower stratosphere to the middle mesosphere, whereas the correlation is only moderate when comparing with MIPAS ESA and MIPAS IMK-IAA. In terms of mean relative differences, no significant systematic hemispheric or local time biases were found in the comparisons. With respect to all three correlative data sets, around 14 km ACE-FTS exhibits a consistent negative bias in the range of -3 to -25% , in the middle stratosphere ACE-FTS exhibits a negative bias typically better than -11% , in the upper stratosphere the ACE-FTS negative bias tends to peak near 47 km and is within the range of -7 to -13% , and in the stratopause region relative differences are typically within $\pm 6\%$. Above 62 km, the MIPAS relative differences are typically within $\pm 22\%$, whereas the MLS relative differences remain within -5 and 0%. The result of an ACE-FTS dry bias of ~ 0 to 10% above the hygropause, is opposed to the finding of [12], who reported an ACE-FTS v2.2 wet bias of ~ 3 to 8%.

For N_2O , below 35 km, all three data sets agree reasonably well with ACE-FTS. In this region, comparisons with all three data sets yield very strong correlation, and the MIPAS data sets typically agree with ACE-FTS within

-9 and $+7\%$, and the MLS data agree with ACE-FTS within -21 and $+5\%$. These results are similar to, if not better than, the ACE-FTS v2.2 comparison results of [13]. Above 35 km, where the MLS measurement variance is too large to give reasonable agreement with ACE-FTS, MIPAS ESA and ACE-FTS typically agree within $\pm 10\%$. ACE-FTS has a negative bias with respect to MIPAS IMK-IAA on the order of -10% for NH and for AM data and on the order of 20% for SH and for PM data.

Below 30 km, ACE-FTS HNO_3 typically agrees with all three correlative data sets to within $\pm 10\%$, with standard deviations on the order of 7% near the HNO_3 peak and on the order of 25% at the lowest altitude levels. Above 30 km, ACE-FTS tends to exhibit a positive bias on the order of 10–20%, although the MIPAS ESA mean relative differences reach up to $\sim 40\%$ near 40 km, the upper altitude limit of where MIPAS ESA and ACE-FTS agree well. No significant consistent diurnal or hemispheric biases were found in the ACE-FTS HNO_3 data. These results are in line with the ACE-FTS v2.2 comparison results of [14].

ACE-FTS CO profiles were compared with profiles from MIPAS IMK-IAA and MLS. Near the CO VMR minimum (~ 20 km), all comparisons exhibit weak correlation and relatively high standard deviations. Below the minimum, as CO increases with decreasing altitude, comparisons with MLS continue to exhibit poor agreement, whereas better agreement is exhibited between ACE-FTS and MIPAS.

Throughout the stratosphere, with respect to MIPAS, ACE-FTS CO tends to exhibit a negative bias that reaches -31% , but is on average -9% . In this region, the standard deviations for the winter comparisons were much greater than those for summer due to larger variation in winter CO VMR. In the 55–68 km region, ACE-FTS typically exhibited a positive bias, on the order of 0–18% in the winter, and, in the summer, greater than 100% above ~ 65 km. No significant consistent hemispheric bias was found in the mean relative differences throughout the atmosphere.

Comparisons between ACE-FTS and summer MLS CO data yield poor agreement at most altitude levels. Winter comparisons yield mean relative differences typically within $\pm 10\%$ in the 25–40 km altitude range. This bias is mainly due to larger wintertime concentrations in the SH, due to consistent wintertime descent in the Antarctic vortex. Above 40 km, up into the upper mesosphere, ACE-FTS exhibits an average negative bias of -11% with SH data slightly more negative than the NH by ~ 1 to 5%. However, when comparing with MLS data that excludes the summer months, ACE-FTS exhibits an average negative bias of -17% , with no significant hemispheric bias.

Acknowledgments

This project was funded by the Canadian Space Agency (CSA). The Atmospheric Chemistry Experiment is a Canadian-led mission mainly supported by the CSA. Work at the Jet Propulsion Laboratory was performed under contract with the National Aeronautics and Space Administration.

References

- [1] Bernath PF, McElroy CT, Abrams MC, Boone CD, Butler M, Camy-Peyret C, et al. Atmospheric chemistry experiment (ACE): mission overview. *Geophys Res Lett* 2005;32:L15S01. <http://dx.doi.org/10.1029/2005GL022386>.
- [2] Fischer H, Oelhaf H. Remote sensing of vertical profiles of atmospheric trace constituents with MIPAS limb-emission spectrometers. *Appl Opt* 1996;35:2787–96.
- [3] Fischer H, Birk M, Blom C, Carli B, Carlotti M, von Clarmann T, et al. MIPAS: an instrument for atmospheric and climate research. *Atmos Chem Phys* 2008;8:2151–88. <http://dx.doi.org/10.5194/acp-8-2151-2008>.
- [4] Waters JW, Froidevaux L, Harwood RS, Jarnot RF, Pickett HM, Read WG, et al. The Earth observing system microwave limb sounder (EOS MLS) on the aura satellite. *IEEE Trans Geosci Remote Sens* 2006;44:1075–92. <http://dx.doi.org/10.1109/TGRS.2006.873771>.
- [5] Brasseur GP, Solomon S. In: *Aeronomy of the middle atmosphere: chemistry and physics of the stratosphere and mesosphere*. Dordrecht, The Netherlands: Springer; 2005.
- [6] Semeniuk K, McConnell JC, Jin JJ, Jarosz JR, Boone CD, Bernath PF. N₂O production by high energy auroral electron precipitation. *J Geophys Res* 2008;113:D16302. <http://dx.doi.org/10.1029/2007JD009690>.
- [7] Funke B, López-Puertas M, García-Comas M, Stiller GP, von Clarmann T, Glatthor N. Mesospheric N₂O enhancements as observed by MIPAS on Envisat during the polar winters in 2002–2004. *Atmos Chem Phys* 2008;8:5787–800. <http://dx.doi.org/10.5194/acp-8-5787-2008>.
- [8] Boone CD, Nassar R, Walker KA, Rochon Y, McLeod SD, Rinsland CP, et al. Retrievals for the atmospheric chemistry experiment fourier-transform spectrometer. *Appl Opt* 2005;44:7218–31. <http://dx.doi.org/10.1364/AO.44.007218>.
- [9] Boone CD, Walker KA, Bernath PF. Version 3 retrievals for the atmospheric chemistry experiment fourier transform spectrometer (ACE-FTS), the atmospheric chemistry experiment ACE at 10: a solar occultation anthology. Hampton, Virginia, USA: A. Deepak Publishing; 103–27.
- [10] Rothman LS, Jacquemart D, Barbe A, Chris Benner D, Birk M, Brown LR, et al. The HITRAN 2004 molecular spectroscopic database. *J Quant Spectrosc Radiat Transf* 2005;96:139–204. <http://dx.doi.org/10.1016/j.jqsrt.2004.10.008>.
- [11] Dupuy E, Walker KA, Kar J, Boone CD, McElroy CT, Bernath PF, et al. Validation of ozone measurements from the atmospheric chemistry experiment (ACE). *Atmos Chem Phys* 2009;9:287–343. <http://dx.doi.org/10.5194/acp-9-287-2009>.
- [12] Carleer MR, Boone CD, Walker KA, Bernath PF, Strong K, Sica RJ, et al. Validation of water vapour profiles from the atmospheric chemistry experiment (ACE). *Atmos Chem Phys Discuss* 2008;8:4499–559. <http://dx.doi.org/10.5194/acpd-8-4499-2008>.
- [13] Strong K, Wolff MA, Kerzenmacher TE, Walker KA, Bernath PF, Blumenstock T, et al. Validation of ACE-FTS N₂O measurements. *Atmos Chem Phys* 2008;8:4759–86. <http://dx.doi.org/10.5194/acp-8-4759-2008>.
- [14] Wolff MA, Kerzenmacher T, Strong K, Walker KA, Toohey M, Dupuy E, et al. Validation of HNO₃, ClONO₂, and N₂O₅ from the atmospheric chemistry experiment fourier transform spectrometer (ACE-FTS). *Atmos Chem Phys* 2008;8:3529–62. <http://dx.doi.org/10.5194/acp-8-3529-2008>.
- [15] Clerbaux C, George M, Turquety S, Walker KA, Barret B, Bernath P, et al. CO measurements from the ACE-FTS satellite instrument: data analysis and validation using ground-based, airborne and spaceborne observations. *Atmos Chem Phys* 2008;8:2569–94. <http://dx.doi.org/10.5194/acp-8-2569-2008>.
- [16] Sheese PE, Boone C, Walker KA. Detecting physically unrealistic outliers in ACE-FTS atmospheric measurements. *Atmos Meas Tech* 2015;8:741–50. <http://dx.doi.org/10.5194/amt-8-741-2015>.
- [17] Raspollini P, Carli B, Carlotti M, Ceccherini S, Dehn A, Dinelli BM, et al. Ten years of MIPAS measurements with ESA Level 2 processor V6 –Part 1: retrieval algorithm and diagnostics of the products. *Atmos Meas Tech* 2013;6:2419–39. <http://dx.doi.org/10.5194/amt-6-2419-2013>.
- [18] von Clarmann T, Höpfner M, Kellmann S, Linden A, Chauhan S, Funke B, et al. Retrieval of temperature, H₂O, O₃, HNO₃, CH₄, N₂O, ClONO₂ and ClO from MIPAS reduced resolution nominal mode limb emission measurements. *Atmos Meas Tech* 2009;2:159–75. <http://dx.doi.org/10.5194/amt-2-159-2009>.
- [19] Tikhonov AN. On the solution of incorrectly stated problems and a method of regularization. *Dokl Acad Nauk SSSR* 1963;151:501.
- [20] Livesey NJ, Van Snyder W, Read WG, Wagner PA. Retrieval algorithms for the EOS microwave limb sounder (MLS). *IEEE Trans Geosci Remote Sens* 2006;44:1144–55. <http://dx.doi.org/10.1109/TGRS.2006.872327>.
- [21] Rodgers CD. *Inverse methods for atmospheric sounding*. World Sci: Hackensack, New Jersey, USA; 2008.
- [22] Livesey NJ, Read WG, Froidevaux L, Lambert A, Manney GL, Pumphrey HC, et al. EOS MLS Version 3.3/3.4 Level 2 data quality and description document, 2013, Tech. Rep. JPL D-33509, Jet Propulsion Laboratory; Pasadena, CA, USA, Available at (<http://mls.jpl.nasa.gov>).
- [23] Sheese PE, Walker KA, Boone CD, Bernath PF, Funke B. Nitrous oxide in the atmosphere: first measurements of a lower thermospheric source. *Geophys Res Lett* 2016;43:2866–72. <http://dx.doi.org/10.1002/2015GL067353>.
- [24] Manney GL, Santee ML, Rex M, Livesey NJ, Pitts MC, Veefkind P, et al. Unprecedented Arctic ozone loss in 2011. *Nature* 2011;478:469–75. <http://dx.doi.org/10.1038/nature10556>.